Biosensors and Bioelectronics 134 (2019) 90–96

Contents lists available at ScienceDirect

Biosensors and Bioelectronics

journal homepage: www.elsevier.com/locate/bios

LSPR based optical fiber sensor with chitosan capped gold nanoparticles on BSA for trace detection of Hg (II) in water, soil and food samples

Kapil Sadani[a,b], Pooja Nag[a,c], Soumyo Mukherji[a,*]

[a] Department of Biosciences and Bioengineering, Indian Institute of Technology Bombay, Mumbai 400076, India
[b] Department of Instrumentation and Control, Manipal Institute of Technology, Manipal Academy of Higher Education, Manipal 576104, India
[c] Department of Mechatronics Engineering, Manipal Institute of Technology, Manipal Academy of Higher Education, Manipal 576104, India

ARTICLE INFO

Keywords:
Hg (II) Sensor
Localized surface plasmon resonance
U-bend Optical fiber
Bovine serum albumin
Chitosan capped gold nanoparticles
Hg (II) toxicity

ABSTRACT

Mercury is a diversely bioaccumulating heavy metal pollutant toxic to all life forms. In this work, an optical biosensor has been developed and calibrated for universal detection and quantification of mercuric ions, in the range 0.1–540 parts per billion, in biological and environmental samples. Chitosan capped gold nanoparticles on bovine serum albumin are proposed as an ultrasensitive plasmonic mercury receptor on U-bend optical fiber platform. The sensor was calibrated and tested with tap water, sewage contaminated water, marine water, long lived sea fish tissue, fossil fuel fly ash contaminated soil and vegetable samples. The sensor performance was validated with real samples inherently containing mercury. Overall standard error of less than 15% and a coefficient of variation less than 12% (n = 3) was found across all samples, indicating good fitness for diverse usage. Experimentally determined limit of detection of mercuric ions was 0.1 parts per billion in tap water (twenty times lesser than the Environment protection agency limit of 2 parts per billion in drinking water) and 0.2 parts per billion in sea fish and vegetable samples with negligible cross sensitivity towards other metal ions.

1. Introduction

Mercury, in the form Hg (II), is an anthropogenic heavy metal pollutant recirculating in the food chain causing constant bioaccumulation (Selin, 2009). Its degenerative toxicity is well established to all life forms including plants, fishes and animals (Dw, 2000). In humans, it causes motor and cognitive dysfunction, renal impairment, cardiovascular diseases and is a potent carcinogen (Clarkson and Magos, 2006). Mercury influents in the ecosystem are coal fired industries (R. P. Li et al., 2017; R. Li et al., 2017), mines (Gao et al., 2018), cosmetic chemical manufacturing and solid waste incineration. Mercury toxicity in humans is primarily due to consumption of long living marine fishes (Martínez-Salcido et al., 2018), plant products cultivated around coal fired industries, and water from sewage impacted water bodies. It is thus of great significance to develop materials and sensing systems capable of selectively quantifying mercury in complex specimens such as seafood, vegetables and soil, besides surface water.

Various novel receptors such as crown ethers (Fakhari et al., 1997), ionophores (Guo et al., 2006), nucleic acids (Zhu et al., 2012) and proteins (Wang et al., 2012) on a variety of substrates such as plasmonic nanoparticles, hydrogels (Joseph et al., 2011) and polymers have been investigated for detection of mercury. High surface area and enhanced catalytic/electronic properties have made 2D materials such as graphene and phosphorus black promising substrates for ultrasensitive heavy metal sensors (P. R. Li et al., 2017; P. Li et al., 2017). Turn on fluorescence based mercury detection has been extensively studied using Rhodamine B (Huang and Chang, 2006), glucosamine quinolone complexes (Ou et al., 2006), thymine ensemble etc. (Tang et al., 2006; Lippard and Nolan, 2008). Hg-Au/Ag amalgams have long been studied for colorimetric and surface plasmon resonance (SPR) platforms (Rex et al., 2006; Deng et al., 2013). Colorimetric sensors offer the simplest sensing solution but most of them are plagued by relatively high detection limits and cumbersome sample preparation. On the other hand, surface-enhanced Raman spectroscopy (SERS), fluorescence and surface plasmon resonance (SPR) based sensors (Verma and Gupta, 2015) require sophisticated laboratory based instrumentation. Field effect transistors (FETs) (R. Li et al., 2017; P. Li et al., 2017), gratings (Zhang et al., 2018), localized surface plasmon resonance (LSPR) based fiber optics are emerging as promising field deployable transduction platforms. Optical fiber based sensors offer several advantages such as immunity to electromagnetic and electrostatic interferences, compactness, and ease of operability (Christopher et al., 2018; Mishra et al., 2013).

Despite such intensive research on materials and transduction

* Corresponding author.
E-mail address: mukherji@iitb.ac.in (S. Mukherji).

https://doi.org/10.1016/j.bios.2019.03.046
Received 23 January 2019; Received in revised form 13 March 2019; Accepted 21 March 2019
Available online 22 March 2019
0956-5663/

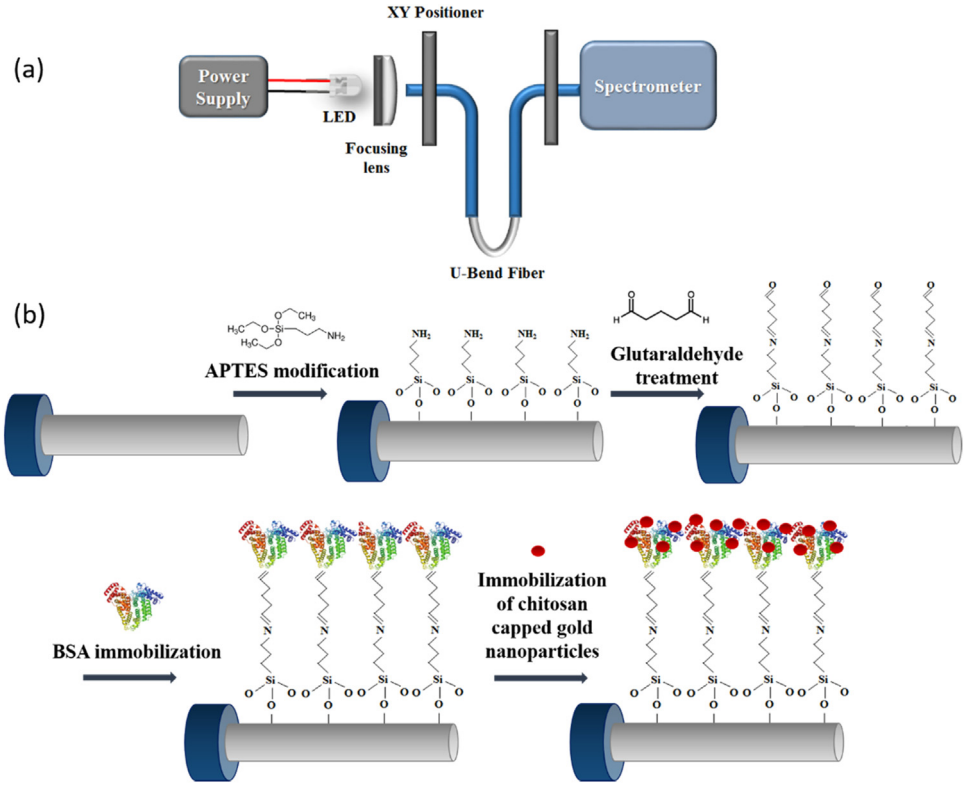

Fig. 1. (a) Benchtop detection assembly (b) U bend optical fiber preparation (i) amine functionalization using APTES (ii) glutaraldehyde crosslinking (iii) BSA immobilization on glutaraldehyde (iv) immobilization of ChGnP on BSA.

methodologies, inductively coupled plasma mass spectroscopy (ICP-MS), atomic emission spectroscopy (ICP-AES) and flameless atomic absorption spectroscopy remain the gold standard in detection of heavy metal ions. These have been studied by Koelmel and Amarasiriwardena (2012), Rao et al. (2002) and Daşbaşi et al. (2016) for heavy metal quantification on various organic analyte matrices. Very few devices for heavy metal detection have made it to the commercial arena (Wei et al., 2014). Possible bottlenecks in field deployability are cumbersome sample preparation, requirement of skilled operator, sensor cross sensitivity and fragility (Maity et al., 2014).

In this work, we report a novel, LSPR based U-bend optical fiber sensor for detection of mercury. Chitosan capped gold nanoparticles (ChGnP) were synthesized and immobilized on bovine serum albumin (BSA) functionalized optical fiber for trace detection of Hg (II) in diverse matrices. The experimental limit of detection of the sensor was found to be 0.1 ppb in tap water which is well below (20 times) the EPA limit of 2 ppb in drinking water. The sensor was calibrated separately for each analyte matrix i.e., tap water, sewage impacted lake water, marine water, digested fish and vegetable samples, washed and digested soil. Validation studies were performed with different mercury contaminated water, soil, vegetable and fish samples collected across India. All samples were analysed by the analytical gold standard method: Inductively Coupled Plasma- Atomic Emission Spectroscopy and Inductively Coupled Plasma-Mass Spectroscopy (ICP-AES/MS) and the results of our sensor were found to be in close agreement to that of gold standard. The sensor developed hereby works in tandem with a handheld reader developed by our group (Chandra et al., 2018) earlier for plug and play on site use. This, to the best of our knowledge, is the first Hg (II) sensor for such diverse applications.

2. Materials and methods

2.1. Reagents

Medium molecular weight chitosan, 190–310 kDa (MCh), gold (III) chloride solution, glutaraldehyde solution, (3-Aminopropyl)triethoxysilane (APTES) and glacial acetic acid were procured from Sigma Aldrich. Bovine serum albumin (BSA) was purchased from GeNei-Merck. Phosphate buffer saline (PBS) of pH 7.8 was prepared using sodium chloride, potassium chloride, disodium hydrogen phosphate and potassium dihydrogen phosphate (SI S5.1). All metal and heavy metal salts were procured from Merck. Deionized water from MilliQ filtration plant was used to prepare all aqueous solutions. All reagents were used without any further purification.

2.2. Synthesis of chitosan capped gold nanoparticles

Polysaccharide mediated synthesis of chitosan capped gold nanoparticles was carried out wherein chitosan was used both as a reducing and stabilizing agent as reported in Huang and Yang (2004) with a few modifications. 3.1 mg/mL MCh was dissolved in fresh deionised water (18.2 MΩ-cm) with 0.4% glacial acetic acid overnight. 300 μL of 25 mM $HAuCl_4$ solution was added to 10 mL of MCh solution in a water bath at 60 °C under continuous magnetic stirring. In about three hours, the solution changed colour from colourless to bright red indicating the formation of gold nanoparticles. The nanoparticles thus synthesized were characterized by field emission gun transmission electron microscope (FEG-TEM) for morphology.

2.3. Optical detection assembly

The optical detection assembly used in this study comprised a broadband white LED (430–700 nm; part no. EDEX-1LA5-E1-AB16) as the input light source, microscope objective (N.A. = 0.65) for focussing,

X-Y positioner (Newport®, USA), SMA 905 connector with bare fiber adapter (Thorlabs®, USA) and USB 4000 spectrophotometer (Ocean Optics) as the detector. High –OH multimode silica optical fibers were cut into 40 cm pieces. 2 cm of the central portion was decladded, cleaned and U-bent as reported earlier (Sai et al., 2009). One end of the fiber was connected to the x-y positioner and the other to the spectrophotometer as illustrated in Fig. 1a. Data acquired using Spectrasuite® software was averaged over 100 samples with an integration time of 50 ms. The U-bend region was incubated in the blank of test analyte matrices to obtain the reference signal and the change in absorbance was recorded by incubating the sensor in analyte matrix known to contain mercuric ions. The governing theory is discussed briefly in SI-S1. All data presented in this article correspond to time resolved absorbance changes at 520 nm (corresponding to the plasmonic peak of ChGnP). All test analyte matrices were regulated in the range of pH between 6.9 and 7.4. All experiments were repeated three times to obtain standard error and coefficient of variation (CV).

2.4. Optical fiber functionalization

Optical fibers were amine functionalized by incubating the U bend region in 1% APTES solution (made in 1 mL ethanol and 0.4 mL acetic acid) for 10 min followed by absolute ethanol rinse and baking at 100 °C for 30 min in a hot air oven. To facilitate amine crosslinking, the fibers were incubated in 3% aqueous glutaraldehyde solution for 30 min and rinsed with deionized water. Thereafter, the fibers were incubated in 2 mg/mL BSA solution in PBS pH 7.8 (SI S5.1) for about 90 min. ChGnP was immobilized on BSA treated optical fiber to an optical density (OD) of 1.2. The functionalized optical fibers were exposed to different analyte matrices spiked with varying concentrations of Hg (II). The sensor was here forth calibrated in the range of 0.1–540 ppb. A schematic of surface functionalization steps is illustrated in Fig. 1b.

3. Results

3.1. Characterization studies

Fourier transform infrared spectroscopy (FTIR) of BSA, ChGnP on BSA and Hg (II) treated ChGnP on BSA was performed with 3000 Hyperion Microscope with Vertex 80 FTIR System, Buker, Germany (Fig. 2). Peaks at 1651 cm^{-1} and 1550 cm^{-1} correspond to -C=O stretch of amide I and N-H bending of amide II. Mercury treatment did not alter these peaks significantly and hence all other peak intensities were normalised with respect to these peaks for further comparison. A broad peak at 3443 cm^{-1} corresponds to –OH and –NH stretch in all the three cases. This peak was significantly reduced on Hg (II) treatment indicating chemisorption of Hg (II) on BSA and ChGnP. Chitosan of animal origin have sulphated glycosaminoglycans (GAGs) as contaminants for which C=S is observed between 1275 cm^{-1} and 1030 cm^{-1} and S=O is seen in between 1225 cm^{-1} and 980 cm^{-1}. The band from 950 cm^{-1} to 1207 cm^{-1} is significantly reduced on Hg (II) treatment. This is due to selective sorption of Hg (II) on sulphur and oxygen of both ChGnP and BSA. Peaks at 2857 cm^{-1} and 2921 cm^{-1} correspond to –C-H symmetric and –C-H asymmetric stretch characteristic of polysaccharides. All of the above inferences are in line with previous FTIR reports of chitosan and BSA (Queiroz et al., 2015; Grdadolnik and Mare, 2001).

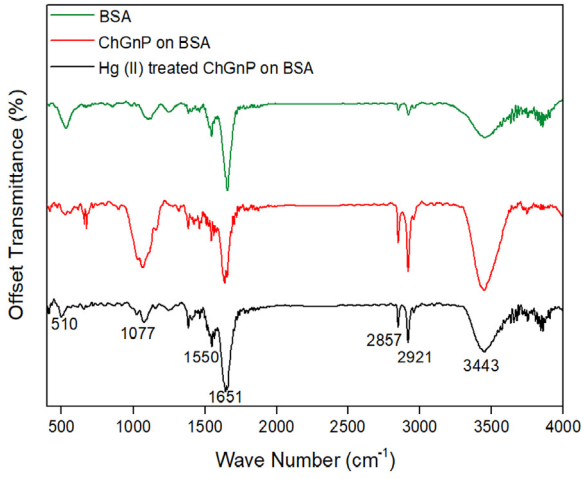

Fig. 2. FTIR (from top to bottom) Bovine Serum Albumin (BSA), Chitosan Capped Gold (ChGnP) on BSA and Hg (II) treated ChGnP on BSA.

Gold nanoparticles were characterized by FEG-TEM, (JEOL-JEM-2100F) for morphology analysis (SI Fig. S2). It was observed that the nanoparticles have clear facets with a mean diameter of approximately 20 nm. Diffraction studies were conducted using Tecnai-G2-F30, FEI. Selected area diffraction showed hexagonal crystalline structure.

Optical fibers were analysed for surface morphology with field emission gun scanning electron microscope JEOL JSM 7600 F. After each functionalization step viz. (i) APTES treatment, (ii) BSA binding, (iii) ChGnP binding and (iv) mercury treatment, the fiber surface was imaged with FEG-SEM as illustrated in SI Fig. S3. The silanized (APTES treated) sensor appeared smooth and uniform throughout. Covalently immobilized BSA were seen as globular structures. The morphology of ChGnP on BSA was similar to that as seen in FEG-TEM. On mercury treatment, the contrast of BSA was enhanced indicating chemisorption of Hg (II) (Watson and Ph, 1958).

3.2. Receptor selection and selectivity studies

Three combinations of materials were analysed on the U bend optical fiber to arrive at the best receptor combination. Each combination of receptors was tested individually with 1 μM each of Hg(II), Pb(II), As (II) and Cu(II) to determine the sensitivity towards heavy metals (Fig. 3a). In the first scheme, citrate capped gold was electrostatically immobilized on silanized U-bend optical fibers. BSA was then immobilized using MUA-EDC/NHS chemistry (SI S5.2). In the second scheme, ChGnP was immobilized on polyanionic Poly(sodium 4-styrenesulfonate) (PSS), coated U bend optical fiber. Neither scheme offered sensitivity nor selectivity towards Hg (II) with respect to other common heavy metals. In a third scheme, fluorescent BSA-Au nanoclusters (AuNC) were synthesized and immobilized (SI-S5.3) on U bend fibers. These were selective to Hg (II) but did not offer desirable sensitivity. ChGnP was then immobilized on BSA (reconstituted in PBS at 7.8 pH) as shown in Fig. 1b. This combination had the highest sensitivity and selectivity towards Hg (II) and was hence selected as the best receptor pair for further studies. Hg (II) was spiked in deionised water to obtain a reference calibration curve, Fig. 3b.

Selectivity of ChGnP on BSA towards Hg (II) was determined by testing the U bend optical fiber sensor with metal ions commonly present in water and food matrices. 1 μM each of Na, K, Mg (II), Mn (II), Cu (II), Fe (III), Zn (II), Pb (II), As (III) and Hg (II) ions dissolved separately in deionized water (Fig. 3c, d), was used for selectivity determination. Also, 1 μM of all metal ions were mixed together and a similar experiment was conducted with and without the presence of mercury in the mixture. Time resolved spectral responses at 520 nm were significantly higher to Hg (II) even in the presence of diverse metal ions after thirty minutes.

3.3. Experiments with tap water

Municipal corporation (tap) water was collected from three cities across India: Durgapur, Kolkata and Mumbai. The samples were analysed by ICP AES/MS and no mercury was found in any sample (SI S6). ChGnP was immobilised on BSA functionalised U bend optical fiber, as

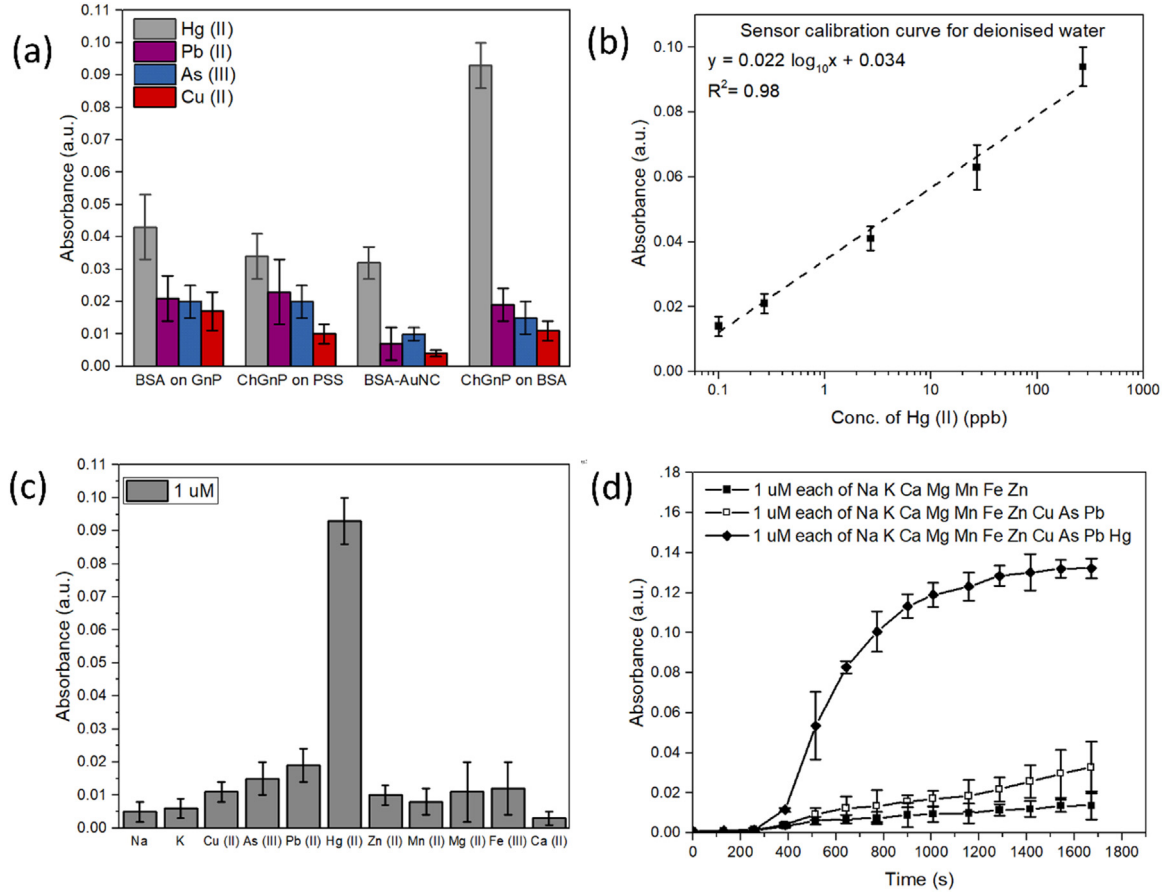

Fig. 3. (a) Selection of optimal receptor combination on the U bend optical fiber for detection of Hg(II): Bovine Serum Albumin on citrate capped gold nanoparticles, chitosan capped gold nanoparticles on Poly(sodium 4-styrenesulfonate), BSA gold nanoclusters and, finally chitosan capped gold nanoparticles on bovine serum albumin. (b) Sensor calibration curve for different concentrations of Hg (II) spiked in deionised water (DI), (c) Selectivity analysis: absorbance change at 520 nm while incubated in 1 μM of individual metal ions dissolved in DI and (d) time resolved spectral response at 520 nm on subjecting the sensor to a mixture of 1 μM each of common metal ions, 1 μM each of common metals and heavy metals without Hg (II) and with Hg (II).

illustrated in schematic Fig. 1b, to an OD of 1.2 for ninety minutes. The absorbance spectrum for the same is shown in Fig. 4a with a LSPR peak at around 530 nm. Hg (II) was spiked in Mumbai tap water and seven serial dilutions in triplicates were made ranging from 0.1 ppb to 540 ppb. A typical spectral response obtained by subjecting the sensor to 27 ppb Hg (II) spiked in Mumbai tap water is illustrated in Fig. 4b. The peak spectral maxima on subjection to Hg (II) is obtained at 520 nm and hence the absorbance changes at 520 nm are considered for sensor calibration. Time resolved spectral responses over 30 min for four different concentrations of Hg (II) (n = 3) is depicted in Fig. 4c. A linear sensor calibration curve (R^2 =0.94) was obtained by plotting the changes in peak spectral response at 520 nm as depicted in Fig. 4d. To validate the sensor calibration across other tap water matrices, recovery studies were performed by spiking 1 ppb and 10 ppb of Hg (II) in tap water from other cities, Durgapur and Kolkata. An overall recovery ranging from 90% to 114% was observed across all tap water samples with a coefficient of variation (C.V. < 9%) as illustrated in Table 1.

A similar set of experiments was performed with marine water collected from two sites along the Arabian Sea and one on the Bay of Bengal, and sewage contaminated Powai lake water, Mumbai. The results are summarised in SI-S7. To validate this sensor calibration across other sea water matrices, recovery studies were conducted by spiking 50 ppb of Hg(II) in sea water collected from sources other than that used for sensor calibration. Recovery was in the range 89–102% with C.V. < 8.3% (Table 1).

3.4. Experiments with washed and digested soil

Soil samples were collected five hundred meters away from three different thermal power plants across India (SI-S2). Soil samples were ground and dried overnight. The samples were acid digested as per EPA 3050B and heavy metal quantification was done using ICP-AES/MS (SI-S6). Soil from IIT-B nursery was collected and characterized for metal content. Since it was not found to contain any Hg (II), it was used as the reference matrix to generate the calibration curve. The digested soil samples were neutralized by using $CaCO_3$ and NaOH (6.9 < pH < 7.4) and final volume was adjusted to 40 mL. A linear (R^2 =0.93) sensor calibration curve was obtained by spiking five different concentrations of Hg (II) (n = 3) in the range from 0.2 ppb to 540 ppb to the digested and neutralized reference matrix, Fig. 5c. Sensor validation studies were performed by comparing Hg (II) as indicated by our sensor to the ICP-MS data of samples characterized to contain Hg (II) (R^2 = 0.99, Fig. 5d, SI S8).

Recovery studies were established by spiking 2 ppb and 10 ppb of Hg (II) in digested IIT-B soil. Recovery was in the range 110–119% with C.V. < 8.2%. To avoid the use of acids and ease outfield deployability by the user directly, a linear (R^2 =0.98) calibration curve was also generated by spiking five different concentrations of Hg (II) in washed and filtered IIT-B nursery soil sample, in the range from 27 ppb to 540 ppb (n = 3), Fig. 5c. Both the detection limit (27 ppb) and time of response (1 h) was found to be higher in the case of washed soil samples as they contained substantially higher particulate and organic matter, diffusion limiting the transduction process.

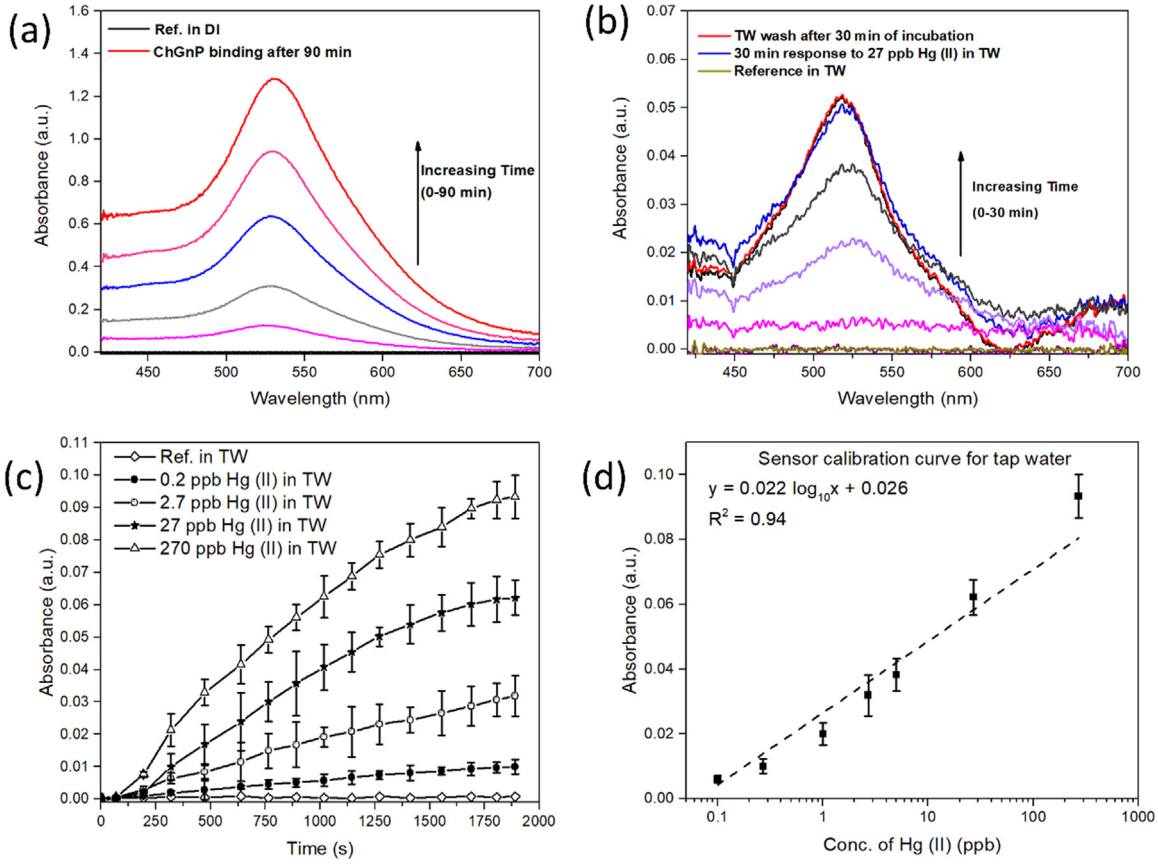

Fig. 4. (a) Absorbance spectrum of ChGnP binding on BSA coated U-bend optical fiber probe (b) absorbance spectrum on subjecting the prepared probe to 27 ppb Hg (II) in tap water (TW) (c) real time absorbance changes to 0.27 ppb, 2.7 ppb, 27 ppb and 27 ppb of Hg (II) in TW (d) sensor calibration curve for Hg (II) in TW (n = 3).

Table 1
Recovery studies of the developed sensor in different liquid analyte matrices.

Sample Details		Fraction of Hg (II) spiked (in ppb)	Fraction of Hg (II) found (in ppb)	Recovery (%)	Coefficient of Variation for n=3 (C.V.)
Tap Water	Hg (II) spiked in Kolkata Municipal Corporation (tap) water	1	0.9	90	7.7
		10	9.3	93	8.3
	Hg (II) spiked in Durgapur MC water	1	1	100	7.4
		10	11.4	114	9
Sewage Contaminated Water	Hg (II) spiked in Powai lake water	2	1.8	90	12.5
		10	8.2	82	8.8
Sea Water	Hg (II) spiked in Puducherry sea water	50	44.8	89	5.8
	Hg (II) spiked in Juhu sea water	50	51.1	102	8.3
Digested Soil Sample	Hg (II) spiked in uncontaminated IITB Nursery soil	2	2.21	110	6.9
		10	11.9	119	8.2

3.5. Experiments with digested fish and vegetables

Fresh sea fish samples of long living sea fishes: kingfish, shark and tuna were procured from local fish market, Mumbai. Vegetable samples, spinach, cabbage, radish and onion, grown in highly industrialised areas were collected for analysis. All samples were cleaned with deionized water and dried overnight. One gram of each sample was measured and microwave digested as described in EPA 3052. The samples were characterized by ICP-MS and ICP-AES to measure metal content (SI S6). The digested samples and blank (mixture of acids used for digestion) were neutralized with NaOH ($6.9 < pH < 7.4$) to a final volume of 20 mL. The neutralized blank was used to derive the sensor calibration curve by spiking four different concentrations of Hg(II) (n = 3) in the range from 0.2 ppb to 270 ppb ($R^2 = 0.98$) (Fig. 5c). Digested food samples inherently containing Hg (II) viz. onion, cabbage, kingfish and shark were used to validate this calibration. Hg (II) as indicated by our sensor in these samples is plotted against that actually found by ICP-MS ($R^2 = 0.99$), Fig. 5d. Overall error was less than 15% with a C.V. < 10% indicating good fitness for diverse usage across all digested organic matrices.

4. Discussion

The unique integration of bovine serum albumin and chitosan capped gold nanoparticles on the U-bend optical fiber platform has been demonstrated as a very stable and repeatable Hg(II) detector across diverse liquid analyte matrices. Chemisorption, electrostatic interactions, hydrophobic and van-der-waals interactions are hypothesized to be the governing factors of sensitivity and selectivity towards Hg (II). Hg (II) is likely to be preferentially chemisorbed on lone pair

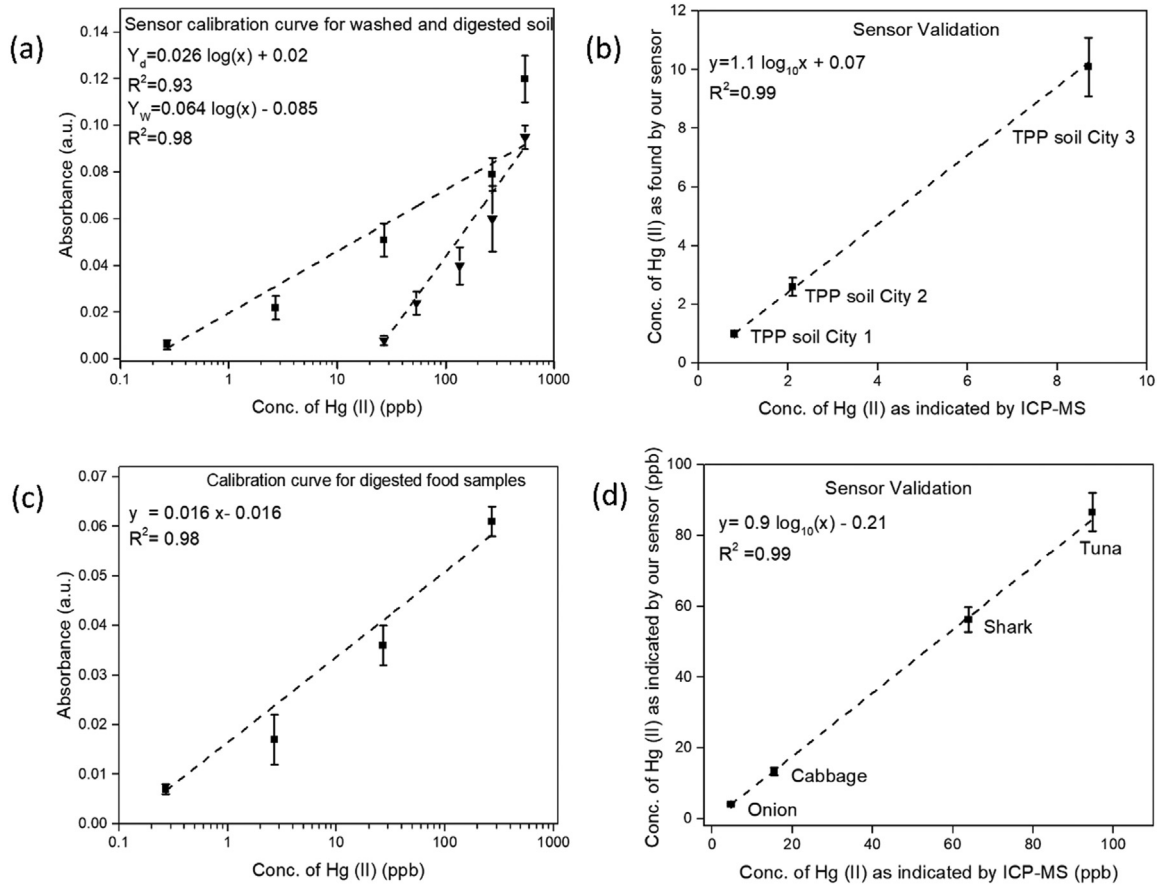

Fig. 5. (a) Sensor calibration curve for Hg (II) in digested and washed soil (b) Sensor validation with digested soil samples inherently containing Hg (II) (SI-S2, SI-S8), samples being collected 500 m from thermal power plants (TTPs) in three different cities across India (c) Sensor calibration curve for Hg(II) in digested food samples (d) validation with digested food samples inherently characterized to contain Hg (II) by ICP-MS.

electrons of nitrogen, oxygen and sulphur in chitosan and BSA. Also, as illustrated in Pearson, 1963, where, Hg (II) acts as the soft acid with a strong affinity towards sulphur and phosphorous containing groups in both chitosan and bovine serum albumin. A significant reduction in –OH and –NH stretch was observed at 3443 cm^{-1} and a decrease in C-O-C bridge intensities at 1021 cm^{-1} and 1077 cm^{-1} on Hg (II) treatment (Fig. 2), confirms the same. Hydrophobic interactions leading to mercury sorption on alpha helix of proteins is well documented (Wei and Dan, 2014). This, also is hypothesized to play a role in Hg (II) detection in the present sensor. For higher mercury concentrations, it is possibly van-der-waals interaction with the thiol groups of BSA that result in complexation with the beta structure of the protein.

The transduction is primarily effected by localized refractive index change in a region of highest available evanescent power SI-S1. Mercury is adsorbed on the nanoparticles themselves and also the layer of protein beneath. Due to the interaction in the plasmonic field, this is recorded as an increase in absorbance at the plasmonic peak of gold nanoparticles (around 520 nm) while adsorption of mercury on the protein monolayer, not in the plasmonic field causes a slight increase in absorbance across all wavelengths. Both of these features can been clearly visualised from Fig. 4b. The sensor proposed here has exceptionally low noise floor. Theoretical limit of detection (LoD) was hence calculated to be 14 ppt as illustrated in SI-S9.

5. Conclusion

LSPR based U-bend optical fiber sensor has been developed in this work for ultrasensitive detection of Hg (II) with a linear range from 0.1 ppb to 540 ppb in tap water. The sensor is inspired from the very causes of bioaccumulation of mercury in life forms, that is, its tendency to form complexes with proteins and its property of behaving as a weak acid, having a strong affinity towards sulphur and phosphorus containing moieties, abundantly present in proteins and polysaccharides of animal origin. The key novelty lies in the use of bovine serum albumin (a protein) and chitosan capped gold nanoparticles for mercuric ion detection; also, the chemistries with which the receptors have been integrated to yield an exceptionally low noise floor sensor. The sensor exhibits negligible cross sensitivity towards other metal and heavy metal ions. The sensor was calibrated separately for tap water, sewage contaminated water, sea water, soil and food samples collected from diverse geographic locations across India. Validation studies were conducted using real sea fish, vegetable and soil matrices, quantified to inherently contain mercury. Recovery analysis was conducted for determining the sensor behaviour in similar matrices of different origin. The sensor performance was robust across the diverse analyte matrices tested (with a detection limit well below that defined by EPA and WHO), a unique technological advancement over existing technologies in research. A limitation which remains for this sensor is the need for mercuric ions to remain in the ionic state for detection. Hence, for detection of mercury in complex organic specimen, digestion of the sample is inevitable (as is the case with gold standard ICP-MS/AES). The sensor works in tandem with a handheld reader developed by our group earlier. With a maximum error of 15% and coefficient of variation of 12% across all samples, the developed sensor is ready for extensive field trials. Potential fields of application of this sensor are diverse ranging from food inspection, water quality monitoring, evaluating occupational exposure to Hg (II) and soil testing.

Acknowledgements

The authors would like to thank Nethaji S, Arvind D, Nandini S, Giriraj S and Rajesh S for their help in sample collection. Authors acknowledge sophisticated analytical instrumentation facility (SAIF-IIT-B) and Central Surface Analytical Facility (ESCA Lab-IIT-B) for providing basic characterization facility: FEG-SEM, FEG-TEM, ICP-AES, ICP-MS, XPS and FTIR.

Declaration of interests

None.

Appendix A. Supporting information

Supplementary data associated with this article can be found in the online version at doi:10.1016/j.bios.2019.03.046.

References

Chandra, S., Dhawangale, A., Mukherji, S., 2018. Hand-held optical sensor using denatured antibody coated electro-active polymer for ultra-trace detection of copper in blood serum and environmental samples. Biosens. Bioelectron. 110, 38–43. https://doi.org/10.1016/j.bios.2018.03.040.

Christopher, C., Subrahmanyam, A., Sai, V.V.R., 2018. Gold sputtered U-bent plastic optical fiber probes as SPR- and LSPR-based compact plasmonic sensors. Plasmonics 13, 493–502. https://doi.org/10.1007/s11468-017-0535-z.

Clarkson, T.W., Magos, L., 2006. The toxicology of mercury and its chemical compounds. Crit. Rev. Toxicol. 36, 609–662. https://doi.org/10.1080/10408440600845619.

Daşbaşi, T., Saçmaci, Ş., Çankaya, N., Soykan, C., 2016. A new synthesis, characterization and application chelating resin for determination of some trace metals in honey samples by FAAS. Food Chem. 203, 283–291. https://doi.org/10.1016/j.foodchem.2016.02.078.

Deng, L., Ouyang, X., Jin, J., Ma, C., Jiang, Y., Zheng, J., Li, J., Li, Y., Tan, W., Yang, R., 2013. Exploiting the higher specificity of silver amalgamation: selective detection of mercury(II) by forming Ag/Hg amalgam. Anal. Chem. 85, 8594–8600. https://doi.org/10.1021/ac401408m.

Dw, B., 2000. Ecological effects, transport, and fate of mercury: a general review. Chemosphere 40, 1335–1351 (doi10).

Fakhari, A.R., Ganjali, M.R., Shamsipur, M., 1997. PVC-Based Hexathia-18-crown-6-tetraone Sensor for Mercury (II) Ions. Anal. Chem. 69, 3693–3696. https://doi.org/10.1021/ac970133b.

Gao, Z.Y., Li, M.M., Wang, J., Yan, J., Zhou, C.C., Yan, C.H., 2018Fb. Blood mercury concentration, fish consumption and anthropometry in Chinese children: a national study. Environ. Int. 110, 14–21. https://doi.org/10.1016/j.envint.2017.08.016.

Grdadolnik, J., Mare, Y., 2001. Bovine Serum Albumin Observed by Infrared Spectrometry . I . Methodology , Structural Investigation , and Water Uptake. Biopolymers 40–53.

Guo, L., Zhang, W., Xie, Z., Lin, X., Chen, G., 2006. An organically modified sol-gel membrane for detection of mercury ions by using 5,10,15,20-tetraphenylporphyrin as a fluorescence indicator. Sens. Actuators, B Chem. 119, 209–214. https://doi.org/10.1016/j.snb.2005.12.009.

Huang, C.C., Chang, H.T., 2006. Selective gold-nanoparticle-based “turn-on” fluorescent sensors for detection of mercury(II) in aqueous solution. Anal. Chem. 78, 8332–8338. https://doi.org/10.1021/ac061487i.

Huang, H., Yang, X., 2004. Synthesis of polysaccharide-stabilized gold and silver nanoparticles: a green method. Carbohydr. Res. 339, 2627–2631. https://doi.org/10.1016/j.carres.2004.08.005.

Joseph, K.A., Dave, N., Liu, J., 2011. Electrostatically directed visual fluorescence response of DNA-functionalized monolithic hydrogels for highly sensitive Hg2+ detection. ACS Appl. Mater. Interfaces 3, 733–739. https://doi.org/10.1021/am101068c.

Koelmel, J., Amarasiriwardena, D., 2012. Imaging of metal bioaccumulation in Hay-scented fern (Dennstaedtia punctilobula) rhizomes growing on contaminated soils by laser ablation ICP-MS. Environ. Pollut. 168, 62–70. https://doi.org/10.1016/j.envpol.2012.03.035.

Li, P., Zhang, D., Jiang, C., Zong, X., Cao, Y., 2017. Ultra-sensitive suspended atomically thin-layered black phosphorus mercury sensors. Biosens. Bioelectron. 98, 68–75. https://doi.org/10.1016/j.bios.2017.06.027.

Li, R., Wu, H., DIng, J., Fu, W., Gan, L., Li, Y., 2017. Mercury pollution in vegetables, grains and soils from areas surrounding coal-fired power plants. Sci. Rep. 7, 1–9. https://doi.org/10.1038/srep46545.

Lippard, S.J., Nolan, E.M., 2008. Tools and tactics for the optical detection of mercuric ion. Chem. Rev. 108, 3443–3480. https://doi.org/10.1021/cr068000q.

Maity, D., Kumar, A., Gunupuru, R., Paul, P., 2014. Colloids and surfaces A: physicochemical and engineering aspects colorimetric detection of mercury (II) in aqueous media with high selectivity using calixarene functionalized gold nanoparticles. Colloids Surf. A Physicochem. Eng. Asp. 455, 122–128. https://doi.org/10.1016/j.colsurfa.2014.04.047.

Martínez-Salcido, A.I., Ruelas-Inzunza, J., Gil-Manrique, B., Nateras-Ramírez, O., Amezcua, F., 2018. Mercury levels in fish for human consumption from the southeast Gulf of California: tissue distribution and health risk assessment. Arch. Environ. Contam. Toxicol. 273–283. https://doi.org/10.1007/s00244-017-0495-5.

Mishra, S.K., Varshney, C., Gupta, B.D., 2013. Sensitivity enhancement of surface plasmon resonance based fiber optic refractive index sensor using an additional layer of zinc oxide. Proc SPIE 8794 87941F. https://doi.org/10.1117/12.2026061. Fifth Eur. Work. Opt. Fibre Sensors.

Ou, S., Lin, Z., Duan, C., Zhang, H., Bai, Z., 2006. A sugar-quinoline fluorescent chemosensor for selective detection of Hg2+ ion in natural water. Chem. Commun. 4392–4394. https://doi.org/10.1039/b607287a.

Queiroz, M.F., Melo, K.R.T., Sabry, D.A., Sassaki, G.L., Rocha, H.A.O., 2015. Does the use of chitosan contribute to oxalate kidney stone formation? Mar. Drugs 13, 141–158. https://doi.org/10.3390/md13010141.

Rao, K.S., Balaji, T., Rao, T.P., Babu, Y., Naidu, G.R.K., 2002. Cadmium and lead in human hair by inductively coupled plasma- atomic emission spectrometry. Spectrochim. Acta Part B At. Spectrosc. 57, 1333–1338.

Rex, M., Hernandez, F.E., Campiglia, A.D., 2006. Pushing the limits of mercury sensors with gold nanorods. Anal. Chem. 78, 445–451. https://doi.org/10.1021/ac051166r.

Sai, V.V.R., Kundu, T., Mukherji, S., 2009. Novel U-bent fiber optic probe for localized surface plasmon resonance based biosensor. Biosens. Bioelectron. 24, 2804–2809. https://doi.org/10.1016/j.bios.2009.02.007.

Selin, N.E., 2009. Global biogeochemical cycling of mercury: a review Noelle Eckley Selin. Annu. Rev. Environ. Resour. 34, 43–63. https://doi.org/10.1146/annurev.environ.051308.084314.

Tang, Y., He, F., Yu, M., Feng, F., An, L., Sun, H., Wang, S., Li, Y., Zhu, D., 2006. A reversible and highly selective fluorescent sensor for mercury(II) using poly(thiophene)s that contain thymine moietiesa. Macromol. Rapid Commun. 27, 389–392. https://doi.org/10.1002/marc.200500837.

Verma, R., Gupta, B.D., 2015. Detection of heavy metal ions in contaminated water by surface plasmon resonance based optical fibre sensor using conducting polymer and chitosan. Food Chem. 166, 568–575. https://doi.org/10.1016/j.foodchem.2014.06.045.

Wang, Y., Yang, H., Pschenitza, M., Niessner, R., Li, Y., Knopp, D., Deng, A., 2012. Highly sensitive and specific determination of mercury(II) ion in water, food and cosmetic samples with an ELISA based on a novel monoclonal antibody. Anal. Bioanal. Chem. 403, 2519–2528. https://doi.org/10.1007/s00216-012-6052-1.

Watson, B.Y.M.L., Ph, D., 1958. Staining of tissue sections for electron microscopy with heavy metals ii . application of solutions containing lead and barium. J. Biophys. Biochem. Cytol. 4. https://doi.org/10.1083/jcb.4.6.727.

Wei, Q., Nagi, R., Sadeghi, K., Feng, S., Yan, E., Ki, S.J., Caire, R., Tseng, D., Ozcan, A., 2014. Detection and spatial mapping of mercury contamination in water samples using a smart-phone. ACS Nano 8, 1121–1129. https://doi.org/10.1021/nn406571t.

Wei, Y., Dan, Z., 2014. Study of the interaction between mercury (II) and. Environ. Toxicol. Pharmacol. 37, 870–877. https://doi.org/10.1016/j.etap.2014.01.021.

Zhang, Y. nan, Zhang, L., Han, B., Gao, P., Wu, Q., Zhang, A., 2018. Reflective mercury ion and temperature sensor based on a functionalized no-core fiber combined with a fiber Bragg grating. Sens. Actuators, B Chem. 272, 331–339. https://doi.org/10.1016/j.snb.2018.05.168.

Zhu, Y., Xu, L., Ma, W., Xu, Z., Kuang, H., Wang, L., Xu, C., 2012. A one-step homogeneous plasmonic circular dichroism detection of aqueous mercury ions using nucleic acid functionalized gold nanorods. Chem. Commun. 48, 11889–11891. https://doi.org/10.1039/c2cc36559f.